



# Freestanding Needle Flower Structure $\text{CuCo}_2\text{S}_4$ on Carbon Cloth for Flexible High Energy Supercapacitors With the Gel Electrolyte

Tian Xie, Jinxiao Xu, Jie Wang, Chuanli Ma, Linghao Su, Fengying Dong and Liangyu Gong\*

College of Chemistry and Pharmaceutical Sciences, Qingdao Agricultural University, Qingdao, China

## OPEN ACCESS

### Edited by:

Tang Wei,  
Xi'an Jiaotong University, China

### Reviewed by:

Bingbing Tian,  
Shenzhen University, China  
Chengxin Peng,  
University of Shanghai for Science  
and Technology, China

### \*Correspondence:

Liangyu Gong  
lygong@163.com

### Specialty section:

This article was submitted to  
Electrochemistry,  
a section of the journal  
Frontiers in Chemistry

Received: 19 December 2019

Accepted: 20 January 2020

Published: 27 February 2020

### Citation:

Xie T, Xu J, Wang J, Ma C, Su L,  
Dong F and Gong L (2020)  
Freestanding Needle Flower Structure  
 $\text{CuCo}_2\text{S}_4$  on Carbon Cloth for Flexible  
High Energy Supercapacitors With the  
Gel Electrolyte. *Front. Chem.* 8:62.  
doi: 10.3389/fchem.2020.00062

A facile hydrothermal approach was adopted to the direct synthesis of bimetallic sulfide ( $\text{CuCo}_2\text{S}_4$ ) on carbon cloth (CC) without binders for the supercapacitor's electrodes. A possible formation mechanism was proposed. The prepared bimetallic electrode exhibited a high specific capacitance ( $C_{sp}$ ) of  $1,312 \text{ F}\cdot\text{g}^{-1}$  at  $1 \text{ A}\cdot\text{g}^{-1}$ , and an excellent capacitance retention of 94% at  $5 \text{ A}\cdot\text{g}^{-1}$  over 5,000 cycles. In addition, the asymmetric supercapacitor ( $\text{CuCo}_2\text{S}_4/\text{CC}//\text{AC}/\text{CC}$ ) exhibited energy density ( $42.9 \text{ wh}\cdot\text{kg}^{-1}$  at  $0.8 \text{ kW}\cdot\text{kg}^{-1}$ ) and outstanding cycle performance (80% initial capacity retention after 5,000 cycles at  $10 \text{ A}\cdot\text{g}^{-1}$ ). It should be noted that the electrochemical performance of a supercapacitor device is quite stable at different bending angles. Two charged devices in series can light 28 red-colored LEDs (2.0 V) for 5 min. All of this serves to indicate the potentially high application value of  $\text{CuCo}_2\text{S}_4$ .

**Keywords:** flexible electrode, nanoneedles,  $\text{CuCo}_2\text{S}_4$ , pseudocapacitance, supercapacitors

## INTRODUCTION

Supercapacitors are extremely valuable for energy storage, owing to their rapid rechargeable ability and extended life cycle (Gao et al., 2015b; He and Chen, 2015). In recent years, they have been widely applied in many fields, such as power backup devices, hybrid electric vehicles, and portable and wearable electronic products (Dong et al., 2015). While flexible electronic products have experienced explosive growth, all electronic devices require flexible and long-life energy storage systems (Hu et al., 2010; Shen et al., 2014; Liu G. et al., 2018). Currently, the main commercial supercapacitors use carbon materials as electrode materials and thus suffer from low-energy density (Dong et al., 2016). Therefore, designing advanced nanostructures with high-energy density and outstanding performance at high-current densities is still given a large amount of attention and holds great appeal (Bao and Li, 2012; Wang et al., 2014; Huang et al., 2016; Xing et al., 2018).

Transition metal compounds, including oxides and sulfides, can provide superior specific capacitance ( $C_{sp}$ ) due to the rapid faraday redox reaction (Guo et al., 2014; Padmanathan and Selladurai, 2014; Pu et al., 2014; Gao et al., 2015b; Moosavifard et al., 2016). However, the maximum capacitance and energy density of these materials are severely limited by the lower electrical conductivity. Among them, transitional bimetallic sulfides can provide a richer redox reaction,

resulting in a generally superior electrochemical performance (Xiong et al., 2015; Sun et al., 2017; Wang J. et al., 2018; You et al., 2018; Dong et al., 2019). For example, Li et al. supported NiCo<sub>2</sub>S<sub>4</sub> nanorods on Ni foam, which displayed a 94.96% capacitive retention over 10,000 cycles (Li M. L. et al., 2018; Li X.-X et al., 2018). At the same time, it has been found that transition bimetallic sulfides also possess rich redox couples and enhance the electronic conductivity (Ai et al., 2016; Wang et al., 2017). In recent years, CuCo<sub>2</sub>S<sub>4</sub> as electrode material has been found to have excellent electronic conductivity, good electrochemical stability, and higher conductivity when compared to its oxide counterparts. In addition, the synergistic effects due to the interaction between diverse metal compounds leads to an enhanced electrochemical energy storage performance, as compared with monometallic sulfides (Shinde et al., 2019). For example, Tian et al. anchored CuCo<sub>2</sub>S<sub>4</sub> to graphene aerogel through solvent thermal reaction with 668 F·g<sup>-1</sup> at 1A·g<sup>-1</sup>. Asymmetrical supercapacitors based on CuCo<sub>2</sub>S<sub>4</sub>/GA exhibit a maximum of 22 Wh·kg<sup>-1</sup> (Tian et al., 2018). Guo et al. prepared Co<sub>2</sub>CuS<sub>4</sub> on graphene nanosheets, which exhibited C<sub>sp</sub> of 1,005 F·g<sup>-1</sup> at 1A·g<sup>-1</sup> (Guo et al., 2016). In addition, designing nanostructures with large surface areas is important for promoting ion transport in electrochemical processes (Wang et al., 2016; Shang et al., 2018).

In order to adapt to the trend of wearable and flexible supercapacitors, others found it desirable to prepare electrode materials on flexible substrates (Dingshan et al., 2015; He et al., 2018). According to previous reports, carbon fiber, nickel foam, and copper foam are widely applied as conductive substrate (Martti et al., 2009; Yang et al., 2014; Xiao et al., 2015; Sun et al., 2016). Among them, the carbon fiber cloth is considered to be an ideal conductive substrate due to its flexibility, electrical conductivity, and low cost. At the same time, directly growing nanostructured materials on carbon cloth avoids the use of binders, resulting in rapid electro transport (Jiang et al., 2011; Liu et al., 2011; Yuan et al., 2012; Zhang et al., 2012, 2016; Wang et al., 2013).

Here, we confirm that carbon cloth is a conductive substrate that can be used to grow a novel 3D needle-flowerlike CuCo<sub>2</sub>S<sub>4</sub> nanostructure. As a result, the flowerlike CuCo<sub>2</sub>S<sub>4</sub> nanostructure exhibits excellent performance (1,312 F·g<sup>-1</sup> at 1 A·g<sup>-1</sup>). Beyond that, an asymmetric solid-state device was manufactured. As a result, it's provided a significant energy density of 42.9 Wh·kg<sup>-1</sup> with an initial capacitance retention rate of 80%—even after 5,000 cycles in the 1.6 V-wide working potential window, showing excellent cycling stability.

## MATERIALS AND METHODS

### Preparation of CuCo<sub>2</sub>S<sub>4</sub>/CC

All reagents were analytical-grade and used without any additional purification. The carbon cloth was purchased from Ce Tech WOS1009. First, a piece of carbon cloth was refluxed at 100°C for 1 h with HNO<sub>3</sub> and subsequently rinsed with deionized water and ethanol. As is typical, CuCl<sub>2</sub>·6H<sub>2</sub>O (2 mmol), CoCl<sub>2</sub>·2H<sub>2</sub>O (4 mmol), urea (30 mmol), and NH<sub>4</sub>F (20 mmol) were dissolved into 60 mL DI water and stirred for 10 min. Then, the mixture solution and the treated CC were transferred

into 100 mL autoclave. After the hydrothermal reaction (140°C for 6 h), the precursors on carbon cloth were washed with deionized water and ethanol, and then dried at 60°C for 12 h.

Next, thioacetamide (TAA, 5 mmol) was dissolved in 60 mL of absolute ethanol with stirring. Then, the solution and the as-obtained precursor were transferred together to the 100 ml autoclave (140°C for 6 h). Finally, after being washed and dried at 60°C overnight, the carbon cloth of uniform load CuCo<sub>2</sub>S<sub>4</sub> was obtained. The loading mass of CuCo<sub>2</sub>S<sub>4</sub> was about 2.3 mg·cm<sup>-2</sup>. For comparison, CuCo<sub>2</sub>S<sub>4</sub> was directly obtained without the placement of a carbon cloth and the CC without the loaded sample is named blank-CC.

### Characterization

X-ray diffraction (XRD) patterns were recorded on a Bruker D8. The morphology of samples was studied by scanning electron microscopy (SEM) (JEOL-7500F, Japan) and transmission electron microscopy (TEM) (HITACHI-7650, Japan). Cycling voltammetry (CV), galvanostatic charge-discharge (GCD), and electrochemical impedance spectroscopy (EIS) were performed with a CHI760E (Shanghai CH, China) electrochemical workstation. Additionally, the cycle life was tested on a CT2001A LAND Battery Test System (LAND, Wuhan, China).

### Electrochemical Measurements

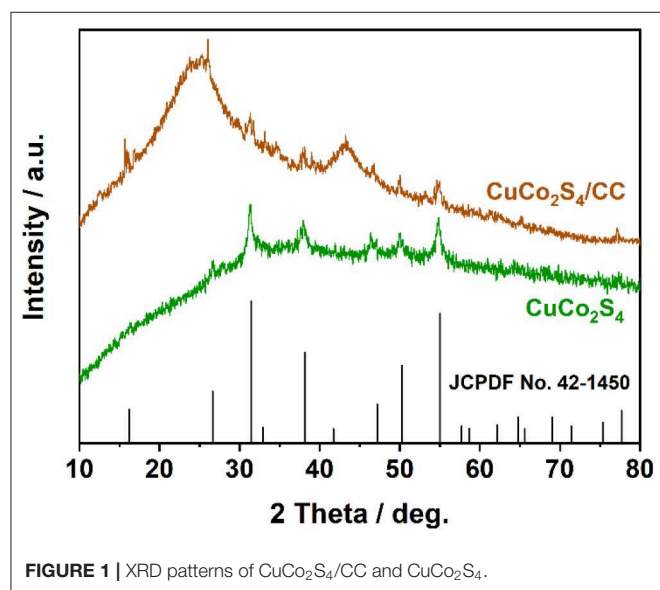
The electrochemical measurements were carried out in a three-electrode system by using 3 M KOH aqueous solution as the electrolyte, where the CuCo<sub>2</sub>S<sub>4</sub>/CC was directly used as the working electrode, Pt foil was used as the counter electrode, and a saturated calomel electrode (SCE.) was used as the reference electrode. The C<sub>sp</sub> of materials was calculated through the equation  $C_{sp} = I \times \Delta t / m \times \Delta V$ , where I,  $\rho$ , m, and V are the discharge current (A), discharge time (s), loading mass (g), and voltage range.

The flexible solid-state asymmetric supercapacitor (FSASC) device was assembled with a CuCo<sub>2</sub>S<sub>4</sub>/CC cathode, active carbon (AC)/CC anode, and PVA/KOH gel electrolyte. The mass ratio between CuCo<sub>2</sub>S<sub>4</sub>/CC and AC/CC was  $m^+/m^- = 0.19$ , according to charge conservation (Yuan et al., 2018). The AC/CC electrode was produced by mixing AC 80 wt%, acetylene black 10 wt%, and PTFE 10 wt% and then coated onto carbon cloth. The PVA/KOH gel electrolyte was maintained by mixing KOH (3 g) and PVA (3 g) in 30 ml DI water at 80°C for 1 h with stirring. The energy and power densities were measured by using equation  $E$  (Wh·kg<sup>-1</sup>) =  $C_{sp} \times \Delta V^2 / 2$  and  $P$  (W·kg<sup>-1</sup>) =  $E / \Delta t$ .

## RESULTS AND DISCUSSION

As illustrated in **Scheme 1**, the CuCo<sub>2</sub>S<sub>4</sub>/CC was successfully synthesized through a simple two-step process. First, the Cu-Co precursor was directly grown on the CC via a hydrothermal process. Subsequently, the Cu-Co precursor is converted into CuCo<sub>2</sub>S<sub>4</sub>/CC via a sulfurization strategy.

The chemical composition is recorded by XRD (**Figure 1**). The different peaks of 16, 26, 31.2, 37.9, 46.9, 49.9, and 54.8° are identical to the standard diffraction data of CuCo<sub>2</sub>S<sub>4</sub> (JCPDS No.42-1450) (You et al., 2018). And the broad peaks at 25 and 45° are derived from the CC substrate (Liu and Wu, 2018).



**Figures 2A–H** shows the topographical changes of  $\text{CuCo}_2\text{S}_4$  on carbon cloth. In **Figure 2A**, the  $\text{CuCo}_2\text{S}_4$  was uniformly adhered to the carbon fiber at a reaction time of 2 h. As seen in **Figure 2E**, the flowerlike structure, composed of acicular  $\text{CuCo}_2\text{S}_4$ , is supported on the carbon fiber. When the reaction time was extended to 4 h (**Figures 2B,F**), the acicular structure of  $\text{CuCo}_2\text{S}_4$  began to aggregate. When the reaction time was 6 h (**Figures 2C,G**), the acicular structure was further aggregated to form a flowerlike structure. The acicular structure provides more active sites, providing abundant pores, while the surface that is initially aggregated by the needle structure provides a larger reaction area. When the reaction time was extended to 8 h, the flowerlike structure supported on the carbon fiber is composed of agglomerated sheets, which reduces the reactive sites and electrochemical performance (**Figures 2D,H**). The

morphological structure of the  $\text{CuCo}$ -pre and  $\text{CuCo}_2\text{S}_4$  is shown in **Figure S1**. In **Figure S1A**, the needle  $\text{CuCo}$ -pre constitutes a flowerlike structure and uniformly grows on the carbon fibers. **Figure S1B** clearly shows the flowerlike  $\text{CuCo}_2\text{S}_4$  structure on the carbon fiber; the exchange of anions during vulcanization does not destroy the overall morphology. In contrast, the  $\text{CuCo}$ -pre and  $\text{CuCo}_2\text{S}_4$  were obtained without adding a carbon cloth substrate (**Figures S1C,D**). It can be seen that both exhibit similar morphologies as those loaded on carbon cloth.

In addition, the microstructure of the  $\text{CuCo}_2\text{S}_4/\text{CC}$  shown by TEM (**Figure 3A**) further demonstrates that the acicular structure of  $\text{CuCo}_2\text{S}_4$  is attached to the carbon fibers. A HRTEM image shows clear lattice fringes with lattice spacing corresponding to the (113) and (004) planes (**Figure 3B**). The SAED in inset indicates the polycrystalline of the materials. Meanwhile, the TEM and SAED image of  $\text{CuCo}_2\text{S}_4$  shows that it is composed of many primary nano-needles and its polycrystalline (**Figures S1E,F**).

Through the above observations, the growth mechanism of flowerlike  $\text{CuCo}_2\text{S}_4$  on carbon cloth can be preliminarily obtained. First, in an alkaline environment,  $\text{Cu}^{2+}$  and  $\text{Co}^{2+}$  ions form a  $\text{CuCo}(\text{OH})_x$  precursor (Wan et al., 2015; Jayaraman et al., 2017). At this time, the solution becomes a supersaturated solution with a large amount of Cu-Co precursor particles. Due to the high surface energy and thermodynamic instability, the nanoparticles adhere to the carbon fibers to reduce the surface energy. Based on the hydrolysis rate control of  $\text{NH}_4\text{F}$ , the precursors will be oriented to grow into the acicular structure and further assemble into a flowerlike structure (Liu S. et al., 2018). The second step is the vulcanization process. The  $\text{S}^{2-}$  released by TAA undergoes anion exchange with  $\text{OH}^-$  to form a  $\text{CuCo}_2\text{S}_4$  flowerlike structure.

The electrochemical properties of  $\text{CuCo}_2\text{S}_4/\text{CC}$  were measured. **Figure 4A** shows the CV curve of  $\text{CuCo}_2\text{S}_4/\text{CC}$ ,  $\text{CuCo}_2\text{S}_4$  and blank-CC at  $10 \text{ mV}\cdot\text{s}^{-1}$ . The curve area of  $\text{CuCo}_2\text{S}_4/\text{CC}$  is larger than that of  $\text{CuCo}_2\text{S}_4$  and blank-CC, which means that  $\text{CuCo}_2\text{S}_4/\text{CC}$  has a higher specific capacitance.

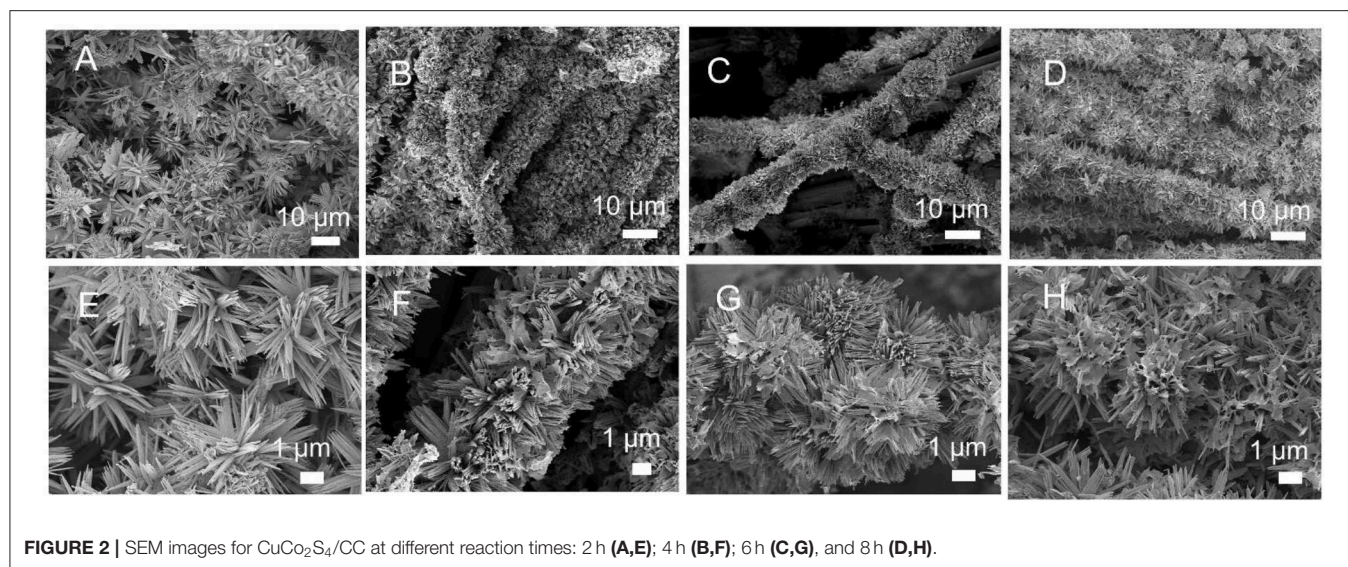


**FIGURE 2** | SEM images for CuCo<sub>2</sub>S<sub>4</sub>/CC at different reaction times: 2 h (A,E); 4 h (B,F); 6 h (C,G), and 8 h (D,H).

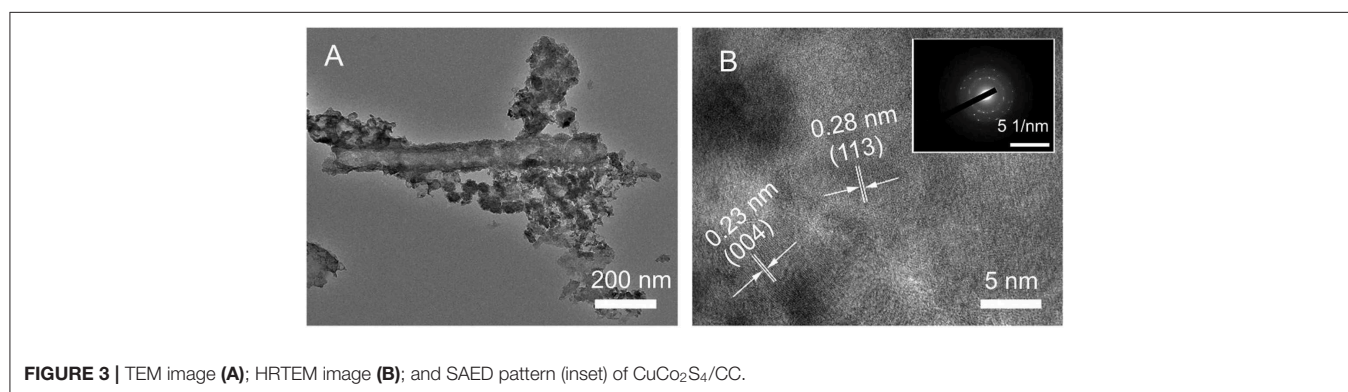


**FIGURE 3** | TEM image (A); HRTEM image (B); and SAED pattern (inset) of CuCo<sub>2</sub>S<sub>4</sub>/CC.

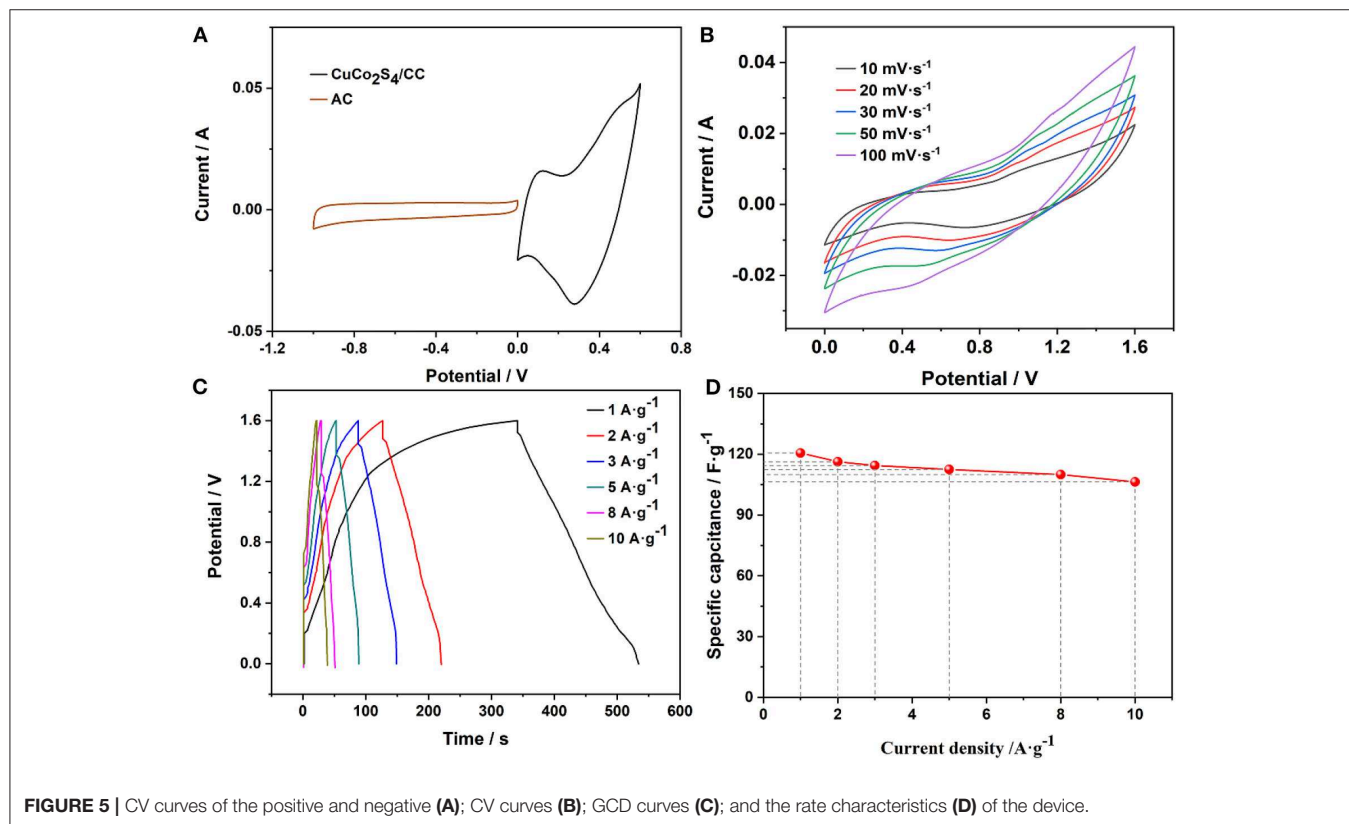
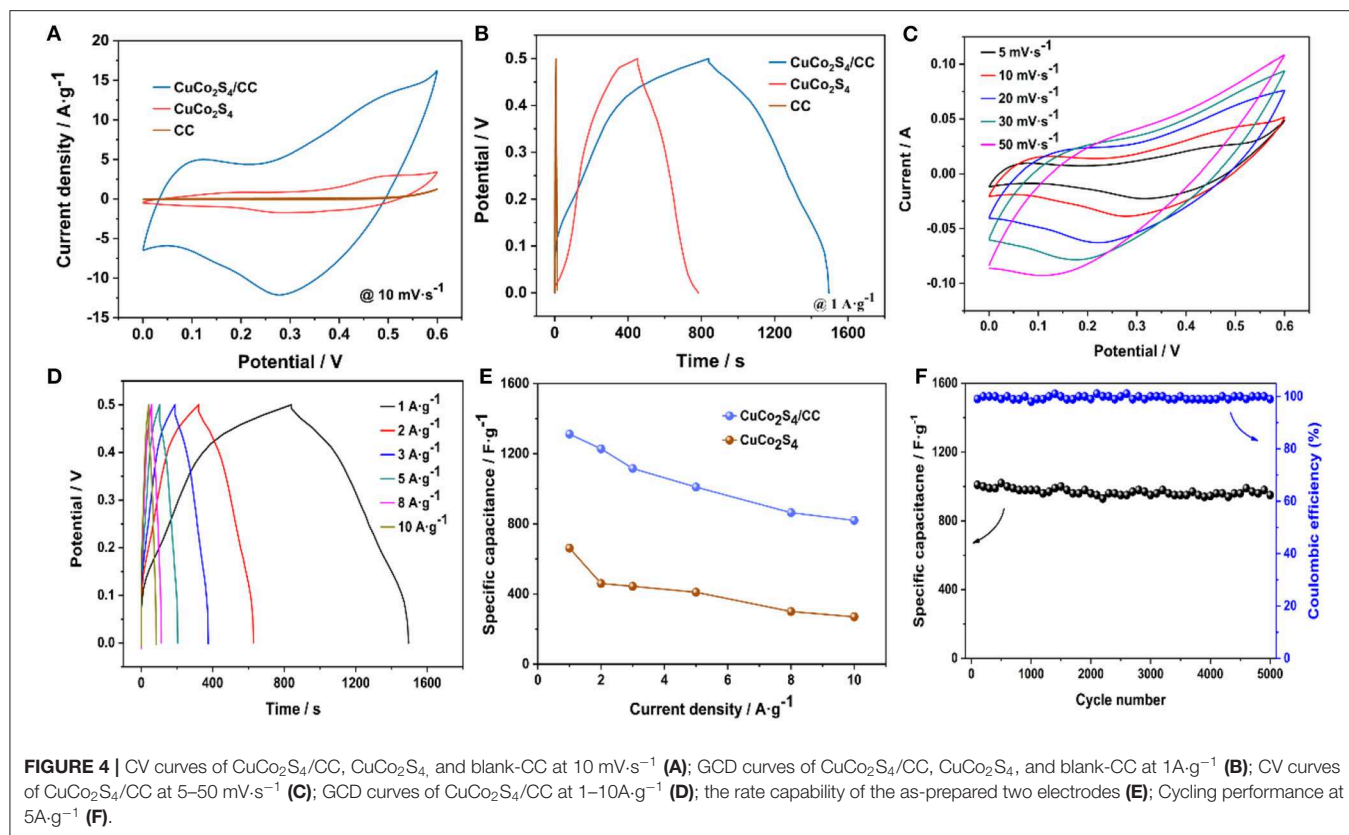
**Figure 4B** is a CuCo<sub>2</sub>S<sub>4</sub>/CC and CuCo<sub>2</sub>S<sub>4</sub> GCD curves at 1 A·g<sup>-1</sup>. Similarly, the discharge time of the CuCo<sub>2</sub>S<sub>4</sub>/CC material is much higher than that of CuCo<sub>2</sub>S<sub>4</sub>. And, the capacitance contribution of blank-CC is negligible. **Figure 4C** shows typical CV curves for CuCo<sub>2</sub>S<sub>4</sub>/CC at 0–0.6 V. Each curve shows a significant redox peak, indicating that the Cu(Co)-S-O/Cu(Co)-S-OH-related faraday reaction was carried out (Jayaraman et al., 2017). As the scan rate increased, the redox peak appeared to shift due to the presence of polarization (Ratha et al., 2017). The possible electrochemical reaction equations are as follows (Kaverlavani et al., 2017; Zhu et al., 2017):

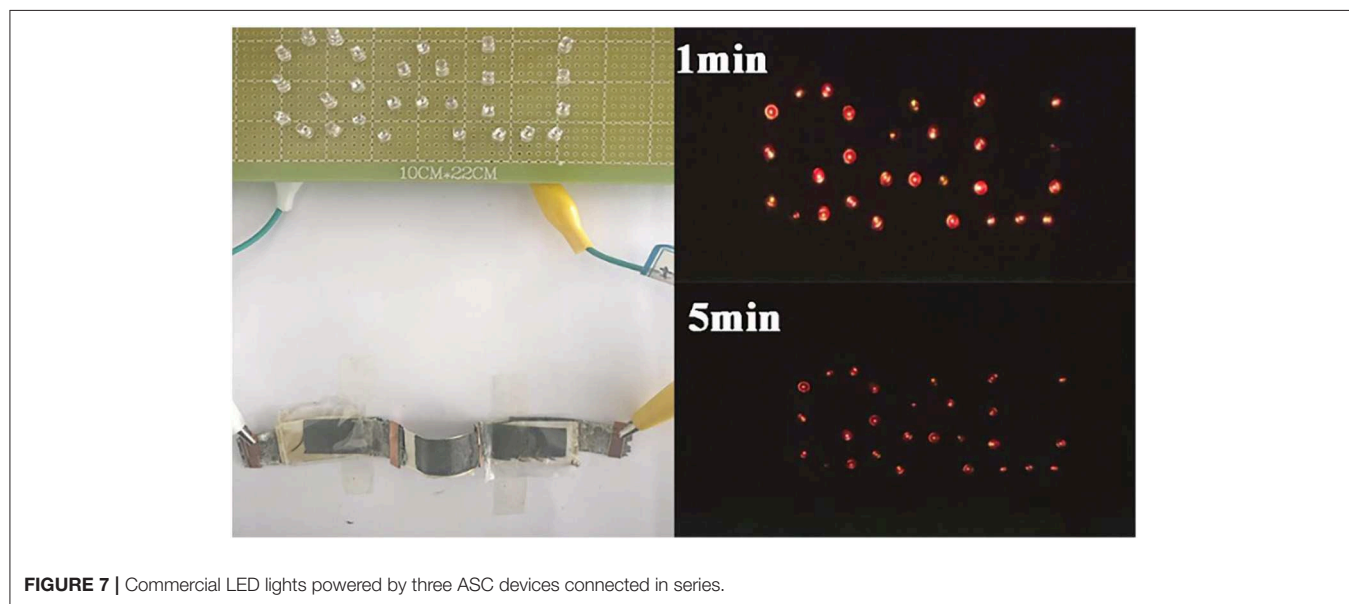
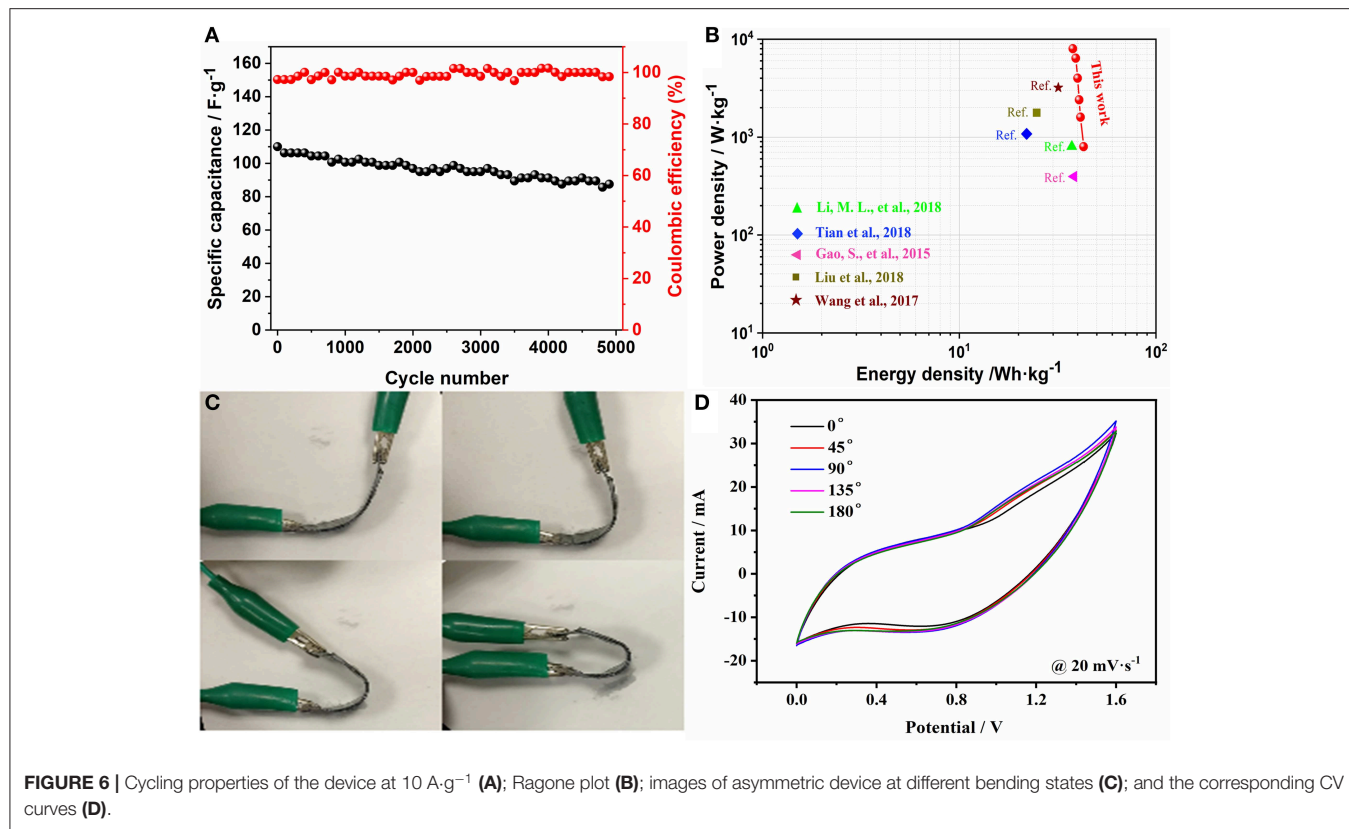


In order to accurately compare the specific capacitances, the exact  $C_{\text{sp}}$  was calculated from GCD measures. **Figure 4D** shows the GCD curves of CuCo<sub>2</sub>S<sub>4</sub>/CC from 1 to 10 A·g<sup>-1</sup>. From the comparison of  $C_{\text{sp}}$  graphs of CuCo<sub>2</sub>S<sub>4</sub>/CC and CuCo<sub>2</sub>S<sub>4</sub> (**Figure 4E**), the discharge-specific capacitance of CuCo<sub>2</sub>S<sub>4</sub>/CC is 1,312, 1,228, 1,116, 1,010, 864, and 820 F·g<sup>-1</sup> at 1, 2, 3, 5,

8, 10 A·g<sup>-1</sup>, which is much larger than CuCo<sub>2</sub>S<sub>4</sub>. The specific capacity values were compatible relative to those previously reported (**Table S1**). On the other hand, lower charge transfer resistance ( $R_{\text{ct}}$ ) and Warburg impedance ( $W$ ) also means that CuCo<sub>2</sub>S<sub>4</sub>/CC can show superior electrochemical performance compared to CuCo<sub>2</sub>S<sub>4</sub> (**Figure S2**). It is noteworthy that the capacities decrease with an increase in current density, which may be due to the fact that the transport and/or diffusion of electrolyte ions are suppressed in high current density (Brousse et al., 2015). The CuCo<sub>2</sub>S<sub>4</sub>/CC electrode maintained an initial capacity of 94% after cycling 5,000 times at 5 A·g<sup>-1</sup>, while the Coulomb efficiency remained almost 100%, indicating excellent cycling stability (**Figure 4F**).

To prove the application potential, the FSASC device was made of CuCo<sub>2</sub>S<sub>4</sub>/CC and AC/CC as the positive and negative electrodes, respectively. **Figure 5A** is the CV curves of CuCo<sub>2</sub>S<sub>4</sub>/CC and AC/CC at 20 mV·s<sup>-1</sup>. The detailed electrochemical data of the AC is shown in **Figure S3**. The electrochemical properties of the assembled FSASC were evaluated. The CV and GCD measurements of the ASC device are shown in **Figures 5B,C**, respectively. At the same time, the charging time of the device is higher than the





discharge time in GCD curves, which may be due to the fact that transport of the electrolyte ion cannot be fully carried out at a low current density (Figure 5C). This phenomenon stems from the nature of the gel electrolyte and the inherent properties of the material (Qi et al., 2015; Wang P. et al., 2018). When the current density is  $10 \text{ A}\cdot\text{g}^{-1}$ , a high  $C_{sp}$

of  $106.3 \text{ F}\cdot\text{g}^{-1}$  can be delivered, which shows a retention of 88.1% (Figure 5D).

The cycle properties of the ASC device were evaluated by cycling 5,000 times at  $10 \text{ A}\cdot\text{g}^{-1}$  (Figure 6A). The  $C_{sp}$  decreases from 110 to  $87.5 \text{ F}\cdot\text{g}^{-1}$ , which exhibits an excellent retention of 80%. Meanwhile, the coulombic efficiency is almost maintained

at 100%, which indicates that the prepared device has excellent performance. **Figure 6B** shows a maximum energy density of  $42.9 \text{ Wh}\cdot\text{kg}^{-1}$  at  $0.8 \text{ kW}\cdot\text{kg}^{-1}$ . And it's still has  $37.8 \text{ Wh}\cdot\text{kg}^{-1}$  at  $8 \text{ kW}\cdot\text{kg}^{-1}$ . In addition, the assembled FSASC device exhibits outstanding flexibility—the CV curves at different angles proving that the bending has little effect on the device (**Figures 6C,D**).

To demonstrate the practical application potential of the equipment, 28 red LEDs assembled in parallel can be illuminated for more than 5 min (**Figure 7**), which indicates that  $\text{CuCo}_2\text{S}_4$  possess excellent energy storage potential.

## CONCLUSIONS

In short, we directly grew needle flower structure  $\text{CuCo}_2\text{S}_4$  on carbon cloth by means of a hydrothermal reaction and vulcanization process; the prepared  $\text{CuCo}_2\text{S}_4/\text{CC}$  shows an excellent electrochemical performance ( $1,312 \text{ F}\cdot\text{g}^{-1}$  at  $1 \text{ A}\cdot\text{g}^{-1}$  and 94% retention over 5,000 cycles). When used as an electrode material for flexible asymmetric supercapacitors, the device provides higher energy density (maximum of  $42.9 \text{ Wh}\cdot\text{kg}^{-1}$ ) and power density (maximum of  $8 \text{ kW}\cdot\text{kg}^{-1}$ ), long-term cycling stability (80% retention over 5,000 cycles), and superior flexibility. The needle flower structure promotes the transport of electrolyte ions, providing a higher specific capacitance. The rapid transport of ions/electrons on carbon fibers imparts high-rate characteristics to flexible solid-state supercapacitors. This indicates that  $\text{CuCo}_2\text{S}_4/\text{CC}$  is promising as a flexible supercapacitor electrode material.

## REFERENCES

- Ai, Z., Hu, Z., Liu, Y., Fan, M., and Liu, P. (2016). Novel 3D flowerlike  $\text{CoNi}_2\text{S}_4/\text{carbon}$  nanotube composites as high-performance electrode materials for supercapacitors. *N. J. Chem.* 40, 340–347. doi: 10.1039/C5NJ02279G
- Bao, L., and Li, X. (2012). Towards textile energy storage from cotton T-shirts. *Adv. Mater.* 24, 3246–3252. doi: 10.1002/adma.201200246
- Brousse, T., Bélanger, D., and Long, J. W. (2015). To be or not to be pseudocapacitive? *J. Electrochem. Soc.* 162, A5185–A5189. doi: 10.1149/2.0201505jes
- Dingshan, Y., Shengli, Z., Wenchao, J., Kunli, G., Li, W., Xudong, C., et al. (2015). Transforming pristine carbon fiber tows into high performance solid-state fiber supercapacitors. *Adv. Mater.* 27, 4895–4901. doi: 10.1002/adma.201501948
- Dong, D., Wu, Z., Wang, J., Fu, G., and Tang, Y. (2019). Recent progress in Co<sub>9</sub>S<sub>8</sub>-based materials for hydrogen and oxygen electrocatalysis. *J. Mater. Chem. A* 7, 16068–16088. doi: 10.1039/C9TA04972J
- Dong, L., Xu, C., Li, Y., Huang, Z.-H., Kang, F., Yang, Q.-H., et al. (2016). Flexible electrodes and supercapacitors for wearable energy storage: a review by category. *J. Mater. Chem. A* 4, 4659–4685. doi: 10.1039/C5TA10582J
- Dong, L., Xu, C., Yang, Q., Fang, J., Li, Y., and Kang, F. (2015). High-performance compressible supercapacitors based on functionally synergistic multiscale carbon composite textiles. *J. Mater. Chem. A* 3, 4729–4737. doi: 10.1039/C4TA06494A
- Gao, S., Liao, F., Ma, S., Zhu, L., and Shao, M. (2015a). Networklike mesoporous  $\text{NiCo}_2\text{O}_4$  grown on carbon cloth for high-performance pseudocapacitors. *J. Mat. Chem. A* 3, 16520–16527. doi: 10.1039/C5TA02876K
- Gao, Z., Yang, W., Wang, J., Song, N., and Li, X. (2015b). Flexible all-solid-state hierarchical  $\text{NiCo}_2\text{O}_4/\text{porous}$  graphene paper asymmetric supercapacitors with an exceptional combination of electrochemical properties. *Nano Energy* 13, 306–317. doi: 10.1016/j.nanoen.2015.02.036

## DATA AVAILABILITY STATEMENT

All datasets generated for this study are included in the article/**Supplementary Material**.

## AUTHOR CONTRIBUTIONS

The manuscript was written through contributions of all authors. All authors have given their approval of the final version of the manuscript.

## FUNDING

This work was financially supported by the Natural Science Foundation of Shandong Province (ZR2017LB031).

## ACKNOWLEDGMENTS

The authors thank the Analytical and Testing Center of Qingdao Agricultural University for allowing them to use its facilities.

## SUPPLEMENTARY MATERIAL

The Supplementary Material for this article can be found online at: <https://www.frontiersin.org/articles/10.3389/fchem.2020.00062/full#supplementary-material>

- Guo, D., Luo, Y., Yu, X., Li, Q., and Wang, T. (2014). High performance  $\text{NiMoO}_4$  nanowires supported on carbon cloth as advanced electrodes for symmetric supercapacitors. *Nano Energy* 8, 174–182. doi: 10.1016/j.nanoen.2014.06.002
- Guo, M., Balamurugan, J., Thanh, T. D., Kim, N. H., and Lee, J. H. (2016). Facile fabrication of  $\text{Co}_2\text{CuS}_4$  nanoparticle anchored N-doped graphene for high-performance asymmetric supercapacitors. *J. Mater. Chem. A* 4, 17560–17571. doi: 10.1039/C6TA07400F
- He, S., and Chen, W. (2015). Application of biomass-derived flexible carbon cloth coated with  $\text{MnO}_2$  nanosheets in supercapacitors. *J. Power Sources* 294, 150–158. doi: 10.1016/j.jpowsour.2015.06.051
- He, Z., Jiang, Y., Li, Y., Zhu, J., Zhou, H., Meng, W., et al. (2018). Carbon layer-exfoliated, wettability-enhanced,  $\text{SO}_3\text{H}^-$  functionalized carbon paper: a superior positive electrode for vanadium redox flow battery. *Carbon* 127, 297–304. doi: 10.1016/j.carbon.2017.11.006
- Hu, L., Pasta, M., Mantia, F. L., Cui, L., Jeong, S., Deshazer, H. D., et al. (2010). Stretchable, porous, and conductive energy textiles. *Nano Lett.* 10, 708–714. doi: 10.1021/nl903949m
- Huang, Z., Zhang, Z., Qi, X., Ren, X., Xu, G., Wan, P., et al. (2016). Wall-like hierarchical metal oxide nanosheet arrays grown on carbon cloth for excellent supercapacitor electrodes. *Nanoscale* 8, 13273–13279. doi: 10.1039/C6NR04020A
- Jayaraman, B., Chao, L., Peera, S. G., Kim, N.H., and Lee, J. H. (2017). High-energy asymmetric supercapacitors based on free-standing hierarchical Co-Mo-S nanosheets with enhanced cycling stability. *Nanoscale* 9, 13747–13759. doi: 10.1039/C7NR03763E
- Jiang, H., Zhao, T., Ma, J., Yan, C., and Li, C. (2011). Ultrafine manganese dioxide nanowire network for high-performance supercapacitors. *Chem. Commun.* 47, 1264–1266. doi: 10.1039/C0CC04134C
- Kaverlavani, S. K., Moosavifard, S. E., and Bakouei, A. (2017). Designing graphene-wrapped nanoporous  $\text{CuCo}_2\text{O}_4$  hollow spheres electrodes

- for high-performance asymmetric supercapacitors. *J. Mater. Chem. A* 5, 14301–14309. doi: 10.1039/C7TA03943C
- Li, M. L., Xiao, K., Su, H., Li, N., Cai, Y. P., Liu, Z. Q., et al. (2018).  $\text{CuCo}_2\text{S}_4$  nanosheets coupled with carbon nanotube heterostructures for highly efficient capacitive energy storage. *ChemElectroChem* 5, 2496–2502. doi: 10.1002/celec.201800329
- Li, X.-X., Wang, X.-T., Xiao, K., Ouyang, T., Li, N., and Liu, Z.-Q. (2018). *In situ* formation of consubstantial  $\text{NiCo}_2\text{S}_4$  nanorod arrays toward self-standing electrode for high activity supercapacitors and overall water splitting. *J. Power Sources* 402, 116–123. doi: 10.1016/j.jpowsour.2018.09.021
- Liu, C., and Wu, X. (2018).  $\text{NiCo}_2\text{S}_4$  nanotube arrays grown on flexible carbon fibers as battery-type electrodes for asymmetric supercapacitors. *Mater. Res. Bull.* 103, 55–62. doi: 10.1016/j.materresbull.2018.03.014
- Liu, G., Wang, B., Liu, T., Wang, L., Luo, H., Gao, T., et al. (2018). 3D self-supported hierarchical core/shell structured  $\text{MnCo}_2\text{O}_4/\text{CoS}$  arrays for high-energy supercapacitors. *J. Mat. Chem. A* 6, 1822–1831. doi: 10.1039/C7TA10140F
- Liu, R., Duay, J., and Lee, S. B. (2011). Heterogeneous nanostructured electrode materials for electrochemical energy storage. *Chem. Commun.* 47, 1384–1404. doi: 10.1039/C0CC03158E
- Liu, S., Yin, Y., Hui, K. S., Hui, K. N., Lee, S. C., and Jun, S. C. (2018). High-performance flexible quasi-solid-state supercapacitors realized by molybdenum dioxide@nitrogen-doped carbon and copper cobalt sulfide tubular nanostructures. *Adv. Sci.* 5:1800733. doi: 10.1002/advs.2018.00733
- Martti, K., Chan, C. K., Ma, J., Yi, C., and George, G. (2009). Printable thin film supercapacitors using single-walled carbon nanotubes. *Nano Lett.* 9, 1872–1876. doi: 10.1021/nl8038579
- Moosavifard, S. E., Fani, S., and Rahmadian, M. (2016). Hierarchical  $\text{CuCo}_2\text{S}_4$  hollow nanoneedle arrays as novel binder-free electrodes for high-performance asymmetric supercapacitors. *Chem. Commun.* 52, 4517–4520. doi: 10.1039/C6CC00215C
- Padmanathan, N., and Selladurai, S. (2014). Controlled growth of spinel  $\text{NiCo}_2\text{O}_4$  nanostructures on carbon cloth as a superior electrode for supercapacitors. *RSC Adv.* 4:8341. doi: 10.1039/c3ra46399k
- Pu, J., Wang, T., Wang, H., Tong, Y., Lu, C., Kong, W., et al. (2014). Direct growth of  $\text{NiCo}_2\text{S}_4$  nanotube arrays on nickel foam as high-performance binder-free electrodes for supercapacitors. *Chempluschem* 79, 577–583. doi: 10.1002/cplu.201300431
- Qi, J. L., Wang, X., Lin, J. H., Zhang, F., Feng, J. C., and Fei, W.-D. (2015). A high-performance supercapacitor of vertically-oriented few-layered graphene with high-density defects. *Nanoscale* 7, 3675–3682. doi: 10.1039/C4NR07284G
- Ratha, S. K., Samantara, A., Singha, K. K., Sadashiv, A., Gangan, Chakraborty, B., et al. (2017). Urea-assisted room temperature stabilized metastable beta- $\text{NiMoO}_4$  experimental and theoretical insights into its unique bifunctional activity toward oxygen evolution and supercapacitor. *ACS Appl. Mater. Interfaces* 9, 9640–9653. doi: 10.1021/acsami.6b16250
- Shang, Y., Xie, T., Ma, C., Su, L., Gai, Y., Liu, J., et al. (2018). Synthesis of hollow  $\text{ZnCo}_2\text{O}_4$  microspheres with enhanced electrochemical performance for asymmetric supercapacitor. *Electrochim. Acta* 286, 103–113. doi: 10.1016/j.electacta.2018.08.025
- Shen, L., Che, Q., Li, H., and Zhang, X. (2014). Mesoporous  $\text{NiCo}_2\text{O}_4$  nanowire arrays grown on carbon textiles as binder-free flexible electrodes for energy storage. *Adv. Funct. Mater.* 24, 2630–2637. doi: 10.1002/adfm.201303138
- Shinde, S. K., Ramesh, S., Bathula, C., Ghodake, G. S., Kim, D. Y., Jagdale, A. D., et al. (2019). Novel approach to synthesize  $\text{NiCo}_2\text{S}_4$  composite for high-performance supercapacitor application with different molar ratio of Ni and Co. *Sci. Rep.* 9, 1–10. doi: 10.1038/s41598-019-50165-5
- Sun, H., Xie, S., Li, Y., Jiang, Y., Sun, X., Wang, B., et al. (2016). Large-area supercapacitor textiles with novel hierarchical conducting structures. *Adv. Mater.* 28, 8431–8438. doi: 10.1002/adma.201602987
- Sun, W., Wang, Y., Wu, H., Wang, Z., Rooney, D., and Sun, K. (2017). 3D free-standing hierarchical  $\text{CuCo}_2\text{O}_4$  nanowire cathodes for rechargeable lithium-oxygen batteries. *Chem. Commun.* 53, 8711–8714. doi: 10.1039/C7CC02621H
- Tian, Z., Wang, X., Li, B., Li, H., and Wu, Y. (2018). High rate capability electrode constructed by anchoring  $\text{CuCo}_2\text{S}_4$  on graphene aerogel skeleton toward quasi-solid-state supercapacitor. *Electrochim. Acta* 298, 321–329. doi: 10.1016/j.electacta.2018.12.103
- Wan, H., Liu, J., Ruan, Y., Lv, L., Peng, L., Ji, X., et al. (2015). Hierarchical configuration of  $\text{NiCo}_2\text{S}_4$  nanotube@Ni-Mn layered double hydroxide arrays/three-dimensional graphene sponge as electrode materials for high-capacitance supercapacitors. *ACS Appl. Mater. Interfaces* 7, 15840–15847. doi: 10.1021/acsami.5b03042
- Wang, G., Wang, H., Lu, X., Ling, Y., Yu, M., Zhai, T., et al. (2014). Solid-state supercapacitor based on activated carbon cloths exhibits excellent rate capability. *Adv. Mater.* 26, 2676–2682, 2615. doi: 10.1002/adma.2013.04756
- Wang, J., Liang, J., Wu, J., Xuan, C., Wu, Z., and Guo, X. (2018). Coordination effect of network NiO nanosheet and a carbon layer on the cathode side in constructing a high-performance lithium-sulfur battery. *J. Mater. Chem. A* 6, 6503–6509. doi: 10.1039/C8TA00270C
- Wang, J.-G., Jin, D., Zhou, R., Shen, C., Xie, K., and Wei, B. (2016). One-step synthesis of  $\text{NiCo}_2\text{S}_4$  ultrathin nanosheets on conductive substrates as advanced electrodes for high-efficient energy storage. *J. Power Sources* 306, 100–106. doi: 10.1016/j.jpowsour.2015.12.014
- Wang, P., Zhang, Y., Yin, Y., Fan, L., Zhang, N., and Sun, K. (2018). *In Situ* synthesis of  $\text{CuCo}_2\text{S}_4$ @N/S-doped graphene composites with pseudocapacitive properties for high-performance lithium-ion batteries. *ACS Appl. Mater. Interfaces* 10, 11708–11714. doi: 10.1021/acsami.8b00632
- Wang, Q., Wang, X., Liu, B., Yu, G., Hou, X., Chen, D., et al. (2013).  $\text{NiCo}_2\text{O}_4$  nanowire arrays supported on Ni foam for high-performance flexible all-solid-state supercapacitors. *J. Mat. Chem. A* 1:2468. doi: 10.1039/c2ta01283a
- Wang, Y., Yang, D., Zhou, T., Pan, J., Wei, T., and Sun, Y. (2017). Oriented  $\text{CuCo}_2\text{S}_4$  nanograss arrays/Ni foam as an electrode for a high-performance all-solid-state supercapacitor. *Nanotechnology* 28:465402.
- Xiao, F., Yang, S., Zhang, Z., Liu, H., Xiao, J., Wan, L., et al. (2015). Scalable synthesis of freestanding sandwich-structured graphene/polyaniline/graphene nanocomposite paper for flexible all-solid-state supercapacitor. *Sci. Rep.* 5:9359. doi: 10.1038/srep09359
- Xing, L., Dong, Y., Hu, F., Wu, X., and Umar, A. (2018).  $\text{Co}_3\text{O}_4$  nanowire@NiO nanosheet arrays for high performance asymmetric supercapacitors. *Dalton Trans.* 47, 5687–5694. doi: 10.1039/C8DT00750K
- Xiong, X., Waller, G., Ding, D., Chen, D., Rainwater, B., Zhao, B., et al. (2015). Controlled synthesis of  $\text{NiCo}_2\text{S}_4$  nanostructured arrays on carbon fiber paper for high-performance pseudocapacitors. *Nano Energy* 16, 71–80. doi: 10.1016/j.nanoen.2015.06.018
- Yang, Y., Zhiwei, P., Gunuk, W., Gedeng, R., Xiujun, F., Lei, L., et al. (2014). Three-dimensional thin film for lithium-ion batteries and supercapacitors. *ACS Nano* 8, 7279–7287. doi: 10.1021/nn502341x
- You, H., Zhang, L., Jiang, Y., Shao, T., Li, M., and Gong, J. (2018). Bubble-supported engineering of hierarchical  $\text{CuCo}_2\text{S}_4$  hollow spheres for enhanced electrochemical performance. *J. Mater. Chem. A* 6, 5265–5270. doi: 10.1039/C7TA07890K
- Yuan, C., Li, J., Hou, L., Zhang, X., Shen, L., and Lou, X. W. D. (2012). Ultrathin mesoporous  $\text{NiCo}_2\text{O}_4$  nanosheets supported on Ni foam as advanced electrodes for supercapacitors. *Adv. Funct. Mater.* 22, 4592–4597. doi: 10.1002/adfm.201200994
- Yuan, X., Tang, B., Sui, Y., Huang, S., Qi, J., Pu, Y., et al. (2018).  $\text{CuCo}_2\text{S}_4$  nanotubes on carbon fiber papers for high-performance all-solid-state asymmetric supercapacitors. *J. Mat. Sci. Mat. Elect.* 29, 8636–8648. doi: 10.1007/s10854-018-8878-6
- Zhang, G. Q., Wu, H. B., Hoster, H. E., Chan-Park, M. B., and Lou, X. W. (2012). Single-crystalline  $\text{NiCo}_2\text{O}_4$  nanoneedle arrays grown on conductive

- substrates as binder-free electrodes for high-performance supercapacitors. *Energy Environ. Sci.* 5:9453. doi: 10.1039/c2ee22572g
- Zhang, Y., Hu, Z., An, Y., Guo, B., An, N., Liang, Y., et al. (2016). High-performance symmetric supercapacitor based on manganese oxyhydroxide nanosheets on carbon cloth as binder-free electrodes. *J. Power Sources* 311, 121–129. doi: 10.1016/j.jpowsour.2016.02.017
- Zhu, J., Tang, S., Wu, J., Shi, X., Zhu, B., and Meng, X. (2017). Wearable high-performance supercapacitors based on silver-sputtered textiles with FeCo<sub>2</sub>S<sub>4</sub>-NiCo<sub>2</sub>S<sub>4</sub> composite nanotube-built multitripod architectures as advanced flexible electrodes. *Adv. Ene. Mat.* 7:1601234. doi: 10.1002/aenm.201601234

**Conflict of Interest:** The authors declare that the research was conducted in the absence of any commercial or financial relationships that could be construed as a potential conflict of interest.

Copyright © 2020 Xie, Xu, Wang, Ma, Su, Dong and Gong. This is an open-access article distributed under the terms of the Creative Commons Attribution License (CC BY). The use, distribution or reproduction in other forums is permitted, provided the original author(s) and the copyright owner(s) are credited and that the original publication in this journal is cited, in accordance with accepted academic practice. No use, distribution or reproduction is permitted which does not comply with these terms.